High Voltage CMOS active pixel sensor chip with counting electronics for beam monitoring

Alena Weber, Felix Ehrler, Rudolf Schimassek, Ivan Perić

***Abstract*—This article presents the monolithic active high voltage CMOS (HV-CMOS) pixel sensor HitPix with counting electronics and frame-based readout. It has been developed for high rate ion-beam monitoring, as used e.g. in medical facilities for radiation therapy. The sensor elements are lowly doped n-well in p-substrate diodes. Pixel electronics is implemented within the sensor cathode (n-well). The substrate can be biased to -120 V. This way, a large depletion zone is induced and radiation tolerance is improved. We could show the overall functionality of the sensor by laboratory measurements of the signal response characteristics and threshold distribution. Further, testing the sensor in the medical ion-beam of Heidelberg Ion-beam Therapy Center (HIT) has proven the suitability of this beam monitor approach.**

***Index Terms*—HV-CMOS, monolithic active pixel sensor, high rate beam monitoring, in-pixel hit counting, radiation therapy.**

I. Introduction

External beam radio therapy is a main pillar in the treatment of tumours. The most commonly used form of radiation is photon radiation. More recently heavy ionised particles – such as protons and carbon ions – have been introduced clinically. In contrast to photons, ions penetrate into matter with an energy in the range of 70 to 250 MeV and decelerate continuously as a function of the penetration depth. This process of delivering the dose produces a characteristic depth-dose curve ("Bragg curve").

Figure 1 shows the specific energy deposition (dE/dx) as function of travelling distance in matter. The Bragg-peak in the dE/dx function is a feature that only appears for heavy charged particles. The heavier a particle is, the sharper is the Bragg-peak. The depth in which the Bragg peak is localised depends on the beam energy, which allows focusing high doses directly into the tumour. At the distal end of the Bragg-peak, the delivered dose declines steeply. This and other characteristics of ion-beam define major clinical advantages of particle therapy that makes it a preferable choice for certain types and locations of tumours [1]: a lower integral dose that is administered to healthy tissue.

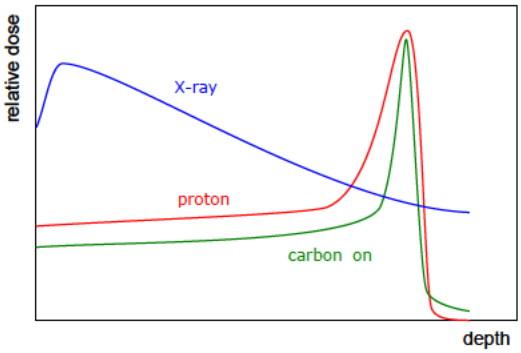

Fig. 1. Energy deposition as a function of penetration depth for different particles. Charged particles have a distinct Bragg-peak. (After [3])

As a consequence, beam monitoring with respect to position and dose is a major corner stone to clinical success in particle therapy. The current beam monitoring system at Heidelberg Ion-beam Therapy Center (HIT) is made of gas-filled ionisation and multi-wire chambers which provide dose, position and spot size information and are connected to the therapy control system.

To fully benefit from high precision dose delivery by scanned ion-beams image guidance is mandatory. In contrast to modern photo based radio therapy, MR based image guidance for ion-beam therapy is technically challenging and is not commercially available, yet.

Within the ARTEMIS (Adaptive RadioThErapie Mit Ionen-Strahlen) project a demonstrator system is under development to implement MRI guided ion-beam delivery including online MR imaging of the target region during irradiation. Specifically, beam control and beam monitoring in the presence of an active MRI device may call for alternative detector technologies, e.g. silicon based semiconductor sensors.

Here we report the design of HitPix ASIC, a pixelated hit-counting silicon sensor implemented in HV-CMOS technology. HV-CMOS sensors combine signal generation in the sensor diode (n-well in p-substrate) with readout electronics (in n-well of the pixel) on the same die. The high depletion voltage increases the depletion zone for large signals and fast charge collection and additionally improves radiation tolerance. [2]

HitPix features several specific design details for operation in an ion-beam: hit-counting pixels, on-chip projection calculation, radiation tolerant design and frame based readout.

This work has been supported by HEiKA - Heidelberg Karlsruhe Strategic Partnership, Heidelberg University, Karlsruhe Institute of Technology (KIT); Germany.

This work has been also supported by Heidelberg Ion Beam Therapy Center (HIT).

The authors acknowledge financial support through the German Federal Ministry of Education and Research (BMBF) within the ARTEMIS project (Grant number: 13GW0436A).

A. Weber was with Karlsruhe Institute of Technology, Karlsruhe, Germany. She is now with Robert Bosch GmbH, Reutlingen, Germany (email: alena.weber@partner.kit.edu).

F. Ehrler is with Heidelberg University Hospital, Heidelberg, Germany and with Karlsruhe Institute of Technology, Karlsruhe, Germany (email: felix.ehrler@kit.edu).

R. Schimassek and I. Perić are with Karlsruhe Institute of Technology, Karlsruhe, Germany.

The exact desired energy of the ion-beam is filtered by a synchrotron. The position and spot size of the beam is to be monitored, as well as the applied dose. This is traditionally done by a redundant pair of multi-wire proportional chambers (MWPC) [4]. This proven technology of gaseous detectors is comparably cheap and reliable, but has some limitations for beam diagnostics: Each layer provides only one projection of the beam profile, two are needed to pin point the beam location. It can not provide information on the two-dimensional beam shape and the resolution is limited by the wire distance which is typically in the order of 0.5 to 1.0 mm. The strong magnetic field of an MRI might influence the movement of the ionised gas in the MWPC leading to an incorrect determination of beam position and the rapidly changing magnetic field might also cause the wires to vibrate, leading to additional uncertainties.

Since position and dose measurement are used to control the irradiation process, they have to be precise and reliable at all times.

A. Beam monitor based on CMOS pixel detector

Silicon based particle tracking sensors with pixels or strips have advantages over MWPCs and are therefore for many years the preferred option in particle tracking devices for high energy physics (HEP) [5], [6]. However, most implementations of silicon tracking sensors are not suited for high rate beam monitoring – they either have too much material (as hybrid pixel detectors) or are not capable of counting particles at high rate (as strip detectors) or are not radiation tolerant enough (as undepleted CMOS pixel sensors).

High voltage CMOS (HV-CMOS) pixel sensors [7] are an exception: These sensors employ commercial HV-CMOS chip production technologies that allow implementation of readout circuits such as particle counters in every pixel and make them capable of sensing high intensity beams. HV-CMOS sensors can be thinned down to 50 µm [8]. HV-CMOS technology is intrinsically more radiation tolerant than other CMOS technologies because they use large and depleted sensor diodes which minimises the charge collection time for signal charge.

Finally, the use of a commercial technology grants low prices and wide availability, allowing also small projects with limited budget to be realised.

B. Advantages of HV-CMOS

Replacing the MWPC stack by a monolithic active pixel sensor designed in HV-CMOS technology promises several advantages:

- Being a pixelated sensor, one layer can replace a two layer stack of MWPCs.
- The dose measurement is already integrated, in two ways [9]: The mere counting of particles of known energy provides directly the dose information and the sensor current can be used to confirm this measurement.
  Consequently, a single layer of an HV-CMOS detector, together with an identical backup layer for fail-save operation, can replace a stack of five MWPCs (two in x-orientation, two in y-orientation, one dose monitor).
- For minimal latency (see next section), a projection of the beam to two sides is the favoured readout option during medical operation. In quality control or scientific operation, individual pixel readout is favoured to obtain a 2D picture of the beam shape.
- Operation of silicon based sensors in a strong magnetic field is standard in HEP [5], [6], therefore they are expected to operate correctly in the vicinity of an MRI.

C. Challenges

There are several challenges and open questions in the beam monitor application which can not be answered from experience with silicon based sensors in HEP.
For ion radiation therapy, protons and carbon ions with moderate energies are used [10]. The energy range is dictated by the required penetration depth and ranges for protons from 48 MeV/u to 221 MeV/u and for carbon ions from 88 MeV/u to 430 MeV/u. The interaction of the latter with silicon is of interest for an HV-CMOS beam monitor. Since HitPix is our first HV-CMOS development for ion-beam monitoring, it has to be studied carefully. Simulation of charged particles passing HV-CMOS sensors are possible, but in the past results have turned out to be not reliable, because of the complex structure of HV-CMOS sensors and because charge collection is not strictly limited to drift or diffusion, but combines both.
Direct monitoring of a particle beam requires a higher rate capability than monitoring secondary particles in HEP.

The radiation tolerance is the most difficult requirement. Unlike particle tracking sensors in HEP, the beam monitor is placed directly in beam. This leads to high and non-uniform doses and fluences. Approximately $6 \cdot 10^{12}/\mathrm{mm}^2$ protons and $6 \cdot 10^{11}/\mathrm{mm}^2$ carbon ions of variable energy pass the sensor per year in the beam center. Both surface total ionising dose (TID) effects and bulk damage due to non-ionising energy loss (NIEL) will occur.

A beam monitor requires a large sensitive area, larger than the maximum size of a single sensor chip. The production steps of HV-CMOS technology are not all performed simultaneously on the whole wafer, but are applied consecutively to limited areas, the reticles. In most cases, reticle size is approximately 2 cm × 2 cm, limited by production tools. Production of larger than reticle devices is possible, but is expensive and has a negative impact on yield: Perfect alignment of adjacent reticles is challenging and typically the parts that need to be combined to form a larger device do not have an identical layout, therefore several tool-sets are necessary. Both alignment and fabrication of diverse tools is costly and contradict one of the major advantages of HV-CMOS sensors over other technologies: the price tag.

In order to anyway obtain a large sensitive area, several individual sensor chips have to be combined minimising dead area between them and without causing inhomogeneities (e.g. gaps between sensors).

D. Counting readout architecture

Beam monitoring does not require identification of individual particles for secondary particle tracking, like in HEP.

For this reason, the use of smart pixels with counting electronics is a good choice for a HV-CMOS beam monitor. Each pixel counts the number of detected particle hits. The states of the counters are read out periodically. One set of counter states is referred to as frame, comparable to a single picture of an imaging sensor.

This readout approach is substantially different to the readout of HV-CMOS particle tracking detectors for HEP: No individual pixel signals are read out, but the number of hits in a certain time interval. Therefore, tracking of particles is impossible (c.f. event pile-up), but also not of interest. The rate capability, on the other hand, is only limited by the analog front-end, the width of the hit counters and the readout bandwidth, all of which can be adjusted by design to a given target application.

By implementing most electronics in the pixels, the periphery of the chip can be small which minimises the insensitive area of the sensor chip. This is favourable in making a beam monitor by abutting of many chips.

As mentioned before, in a medical application safety of the patient is paramount. Therefore, the irradiation has to be interrupted immediately as soon as a deviation from nominal operation (e.g. unintended beam movement) is detected or as soon as the prescribed dose has been administered. The interrupt signal has to be generated within the fraction of a second. Pixelated sensors can meet this timing restriction only if data is being preprocessed on-sensor, to reduce the data bandwidth that has to be transmitted to an aggregating FPGA. Readout of all counter values would take too much time. One solution is that each sensor of a detector generates a projection of the counter data in both directions. This can be realised by adders within each pixel adding its own counter state to the sum of the preceding one. The adders in the last pixel then hold the sum of all pixel counters in this direction, giving the projection of the beam profile. For the final design, two 1D projections will be generated per sensor chip. This information can be read out quickly for real time beam monitoring and interrupt signal generation. Additionally, the collectivity of the 1D projections of all sensors allows for a coarse 2D depiction of the beam.

E. Specifications for the beam monitor

The sensor presented in this paper has been developed for a specific application, the monitoring of the ion-beam of Heidelberg Ion-beam Therapy Center (HIT) [10]. HitPix is a test chip, implementing new concepts and exploring new ideas for a monolithic semiconductor based beam monitor. In its design, specific requirements for HIT have been incorporated. A summary of requirements and corresponding design decisions is listed in table I.

HitPix is not only a technology demonstrator for the ion-beam at HIT, but can also be the basis for the development of beam diagnosis devices for other high rate applications.

[1] 1 mm water equivalent ≈ 0.5 mm silicon

TABLE I
THE MOST IMPORTANT REQUIREMENTS FOR A DETECTOR MONITORING A MEDICAL ION-BEAM (LEFT) AND THE DESIGN DECISIONS MADE TO COMPLY WITH THEM (RIGHT).

Requirement	**Design decision**
Spatial resolution of 200 µm and FWHM resolution of 400 µm	Pixel size is 200 µm × 200 µm
Deviation of beam parameters have to be detected within 100 µs after integration time has been completed	Adaptable frame rate, typical values are in the order of 100 kHz for projection readout
Detector lifetime can not be less than 6 months and should be more than 1 year	HV-CMOS technology and radiation tolerant circuit design are used
Total detector block material budget is 2 mm water equivalent (several sensor layers and mechanical structure)	Thinned sensors are available (100 µm per layer)[1], interconnection via flex PCB, carbon plate for rigidity
Up to 2^{10} particles per second	In-pixel counters store the number of events until frame readout.
Sensitive area has to be at least 25 cm × 25 cm, because of spot size and scanning range.	It can be realised by building a sensor matrix from several sensors (max. 2 cm × 2 cm each), stabilised by a carbon plate and connected via flex PCB.

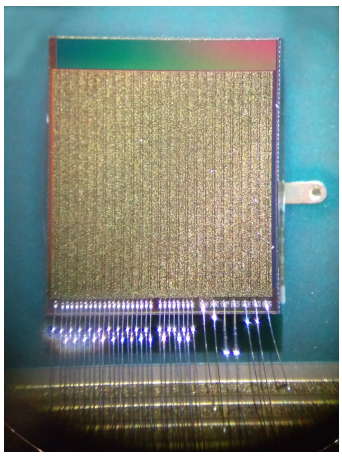

Fig. 2. Photograph of a HitPix chip bonded to the evaluation board.

II. Chip architecture and electronics

The test chip called HitPix has been implemented in a 180 nm HV-CMOS technology. The chip consists of a pixel matrix (24 × 24 pixels) and a small periphery. The sensor area is about 5 mm × 5 mm. The pixel size is 200 µm × 200 µm. A photo of HitPix is shown in figure 2.

A. Pixel

The sensing pixels are diodes formed by deep n-well in lowly doped p-substrate, as used in other HV-CMOS sensors [2]. The p-substrate is reverse biased with high-voltage. In this way, a depletion region of 30 µm to 50 µm depth is generated at the p-side of the sensor junction. The electron-hole pairs generated in the depleted region by particles passing the sensor are separated by the electric field and collected via drift at the deep n-well. The fast charge separation and collection improves tolerance to radiation-induced bulk damage. The tolerance to surface TID effects in the electronics has been

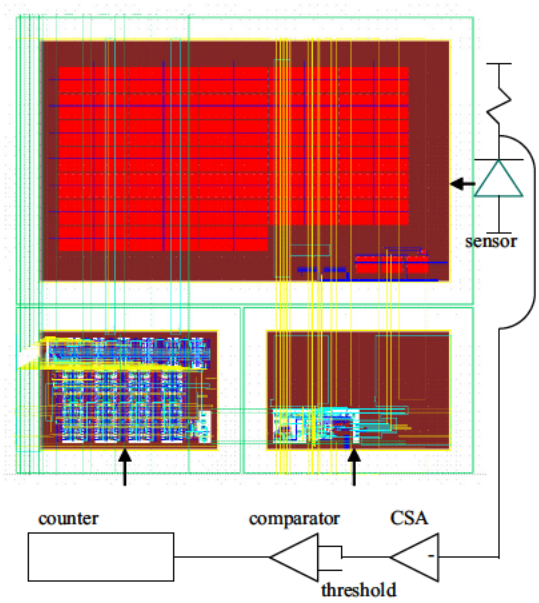

Fig. 3. The layout of the pixel with the three different parts, the sensor electrode (top), the digital (bottom left) and analogue electronics (bottom right).

optimised by special layout techniques: Wherever possible, the more radiation tolerant PMOS circuits are used and all linear NMOS transistors are replaced by enclosed transistors [11, sec. 3.2] [12, sec. 4.2].

The pixel consists of a sensor diode that is connected to a charge sensitive amplifier (CSA). The CSA is AC-coupled to a comparator that compares the CSA output signal with a threshold. The comparator output is connected to the digital circuitry consisting of an 8 bit counter and a 13 bit adder.

Correspondingly, the pixel layout is divided into three parts, the largest one is the sensor electrode. The other parts are the analogue electronics with the CSA and the comparator, and the digital electronics. The layout of a pixel is shown in figure 3. There are two flavours of HitPix, which are described in the following paragraphs.

The baseline version of HitPix has three separated wells in every pixel, one for the sensor diode and one each for analogue and digital electronics, it is referred to as HitPixS, where *S* stands for *separated* wells. Figure 4 shows the schematic cross section of this pixel version. The analogue and digital electronics are embedded in the second deep n-wells occupying 30 % of the pixel. The second n-wells are biased by connecting them to the positive supply rail (Vdd = 1.8 V). The sensor n-well is biased using a bias circuit (R_{bias}) with a high equivalent resistance. This assures that the signal charge flows into the CSA. If a particle ionises the substrate below the second wells, the majority of the signal charge will flow to the positive supply without being amplified and detected. The sensor n-well bias voltage is about 1.8 V, i.e. similar as the voltage of the second n-wells. This reduces possible leakage currents between the sensor well and the secondary wells.

The other chip flavour is called HitPixISO (ISO stands for isolated shallow n-wells). In this chip, the deep n-well used as sensor electrode is surrounding the n- and p-wells housing

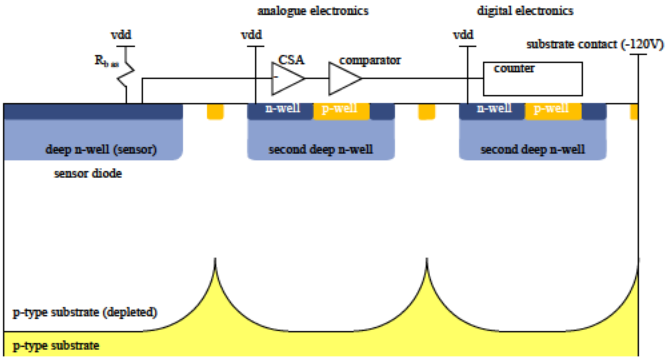

Fig. 4. Cross section of the pixel with separated wells.

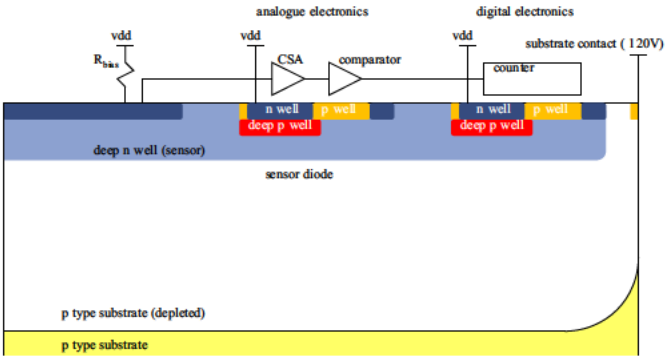

Fig. 5. Cross section of the pixel with large deep n-well and isolated shallow n-wells.

analogue and digital circuits as shown in figure 5. The n-wells containing PMOS transistors are isolated from the deep n-well using extra deep p-wells. This isolation is important to avoid shorting of the sensor n-well with Vdd and to prevent capacitive crosstalk of digital signals to the sensor. The deep p-well has been added to the CMOS process flow. Since in this pixel version there is only one deep n-well for both charge collection and electronics, 100 % of the pixel area is sensitive.

The electronics and layouts of both flavours are identical, the only difference is the shape of the deep n-well, additional deep p-wells and small modifications of the shallow p-wells.

Both HitPix flavours have been produced on substrates with different resistivities, 10 Ωcm and 300 Ωcm. The measurements presented in this manuscript have been performed on 300 Ωcm sensors. A choice of resistivity for the final detector has not yet been made.

B. Analog pixel electronics

Figure 6 shows the transistor level schematics of the charge sensitive amplifier (CSA). The active component of the CSA is a folded cascode amplifier with PMOS input transistor T_{in}. The cascode amplifier has an AC-connection at its input (device C_c), as used in [7]. This allows biasing of the sensor n-well to nearly 1.8 V.

The charge to voltage conversion gain of an ideal CSA is $1/C_f$, where C_f is the feedback capacitance. The gain of a real CSA can be approximated by $1/C_f$ only if its open loop gain is much larger than 1. In the case of our CSA, the loop

gain depends both on the voltage gain of the folded cascode amplifier and on the ratio $C_f/(C_{sens}+C_f)$ where C_{sens} is the capacitance of the sensor diode. Additionally, a small open loop gain reduction arises, because of the voltage division at the capacitance C_c and the gate-source capacitance of T_{in}. In case of a pixel with separated deep n-wells (HitPixS, figure 4), C_{sens} is mainly the junction capacitance of the deep n-well in p-substrate diode. Its simulated value is 52 fF. In case of a pixel with single deep n-well (HitPixISO, figure 5), there is an additional contribution to C_{sens} due to deep n-well to deep- and shallow p-well junction capacitances. Its simulated value is 946 fF.

Figure 7 shows the transistor level schematic of the comparator. It is a standard differential amplifier, w ith o ne input being the signal from CSA and the other input being the threshold. The threshold setting is global (chip-wide). Sensor designs for HEP typically have a local (pixel-wise) threshold adjustment, to be sensitive to sub-MIP signals. This threshold tuning circuit has been assessed unnecessary, since the expected signals from an ion-beam are large. However, irradiation studies have revealed that the different aging speeds of pixels due to inhomogeneous irradiation require actually a stronger threshold adjustment circuit than in HEP where radiation damage is applied more homogeneously. Therefore, we plan to implement threshold adjustment in the next HitPix iteration with a precision of 4 or more bits.

Each pixel contains also a capacitive injection circuit based on the capacitor C_{inj} to generate test signals in each pixel to allow fast testing and commissioning of the sensor chips.

The output of the CSA of one pixel per column is connected to a test pad.

The current consumption of CSA and comparator is adjustable. A typical current through the CSA is 4.7 µA and 2.3 µA through the comparator. The total power consumption per pixel is below 10 µW.

C. Digital pixel electronics

Figure 8 shows the block scheme of the digital part in each pixel. The counter (cnt) is implemented as an 8 bit ripple counter made of 8 cells shown on top of figure 8. The clock input of the first cell ($cell_0$) is driven by the comparator output if the externally generated signal $frame$ is high and if the corresponding pixel row is not addressed for readout ($en_{rowi}=0$). Before reading out the counter states, the bits have to be stored into D-latches by activation of the external signal ld. The counters of all pixels in row i are read out by setting the 5 bit signal $rowaddr$ to i and thus activating en_{rowi}. This connects the outputs of the latches qs to the 8 bit bus $C_0 - C_7$. The logic states of the bus lines (counter states) are loaded into a parallel-in serial-out (PISO) register placed in the chip periphery. In order to select the row from which the data in this register originates, the row address $rowaddr$ is stored in the same register.

For faster readout, an asynchronous adder is implemented in every pixel. From the adders in one column, the sum of counter states in this column is obtained. The adder outputs of the bottom most pixels in every column are connected to the

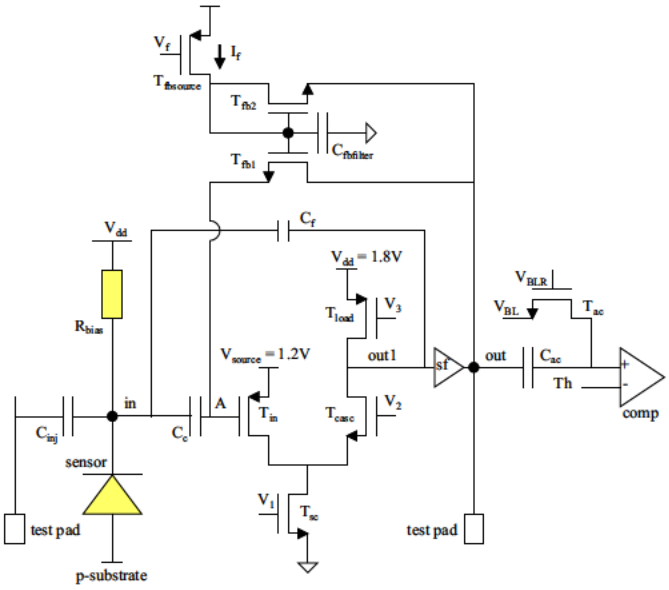

Fig. 6. Schematic of the charge sensitive amplifier with feedback circuit including a continuous reset realised by a current source I_f (After [13]). R_{bias} is implemented with PMOS transistors as shown in [7].

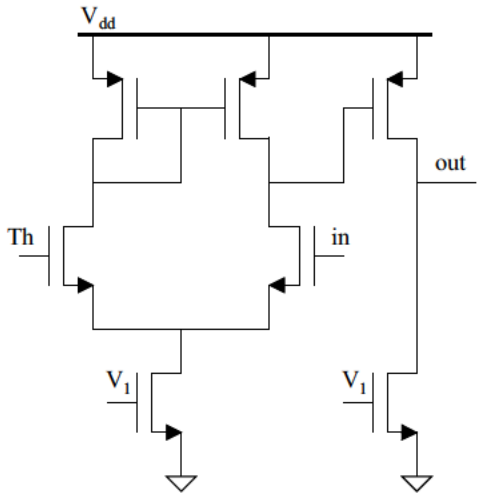

Fig. 7. Schematic of the comparator. [13]

PISO register, too. Using the adders, the column-projection of the beam profile can be read out in just one readout cycle, i.e. by one complete readout cycle of the PISO register. In this way, coarse information about beam position and radiation dose can be read out quickly and can be used to generate an interrupt signal. The 312 bit readout shift register can be operated at up to 75 Mbit/s (The measurements presented in section III were made at 25 and 50 Mbit/s). This feature can also be used in a multi-chip system to optimise the readout of the full beam image. Most of the chips will be outside of the beam. In the first readout step, by reading out the column sums, the position of the beam will be determined. In the second step, all pixel counters in the region of interest can be read out.

Amplifier, comparator and counter have been designed with enclosed NMOS transistors [13]. The enclosed NMOS

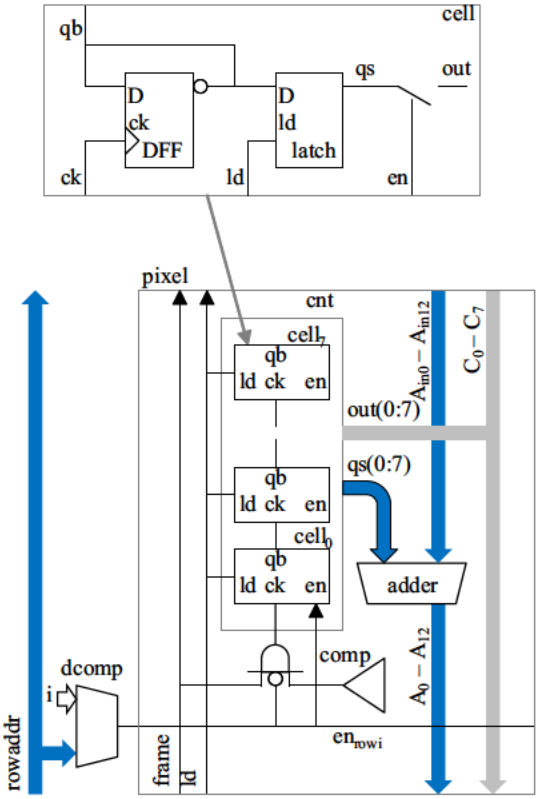

Fig. 8. On the top, the basic element for an 1 bit counter is shown, on the bottom the connection of 8 basic elements to an 8 bit counter. [13]

transistors minimise leakage currents caused by TID [14]–[16].

D. Chip periphery

To minimise the insensitive sensor area, the periphery has to be as small as possible.

The height of the end of column electronics is 128 µm, the width is equal to that of the pixel matrix. The bond pads occupy an additional stripe, 260 µm in height. This means a dead area of approximately $< 15\%$ for HitPix. The periphery area scales with chip width, not with chip height, therefore the fraction of dead area will shrink to $< 2\%$ for a full scale design. The purpose of the periphery is to write out the counter and adder values and to receive configuration bits for the chip. For counter readout, the user selects the row by writing its address into the shift register. The counter values of this row are then loaded and shifted out. Shifting in of control bits and shifting out of counter bits can be done at the same time.

For reading all counter values from the matrix, all rows have to be selected and read out one by one. To read out the row projection provided by the adders, the sum is loaded into the shift register and just one readout cycle is needed.

Data taking can be separated from the readout sequence via a frame signal enabling the counters. The readout can also be done while data taking. The shift register is built from scan flip-flops (scan FF) shown in figure 9. The scan flip-flops are connected to a PISO shift register scheme as shown in figure 10.

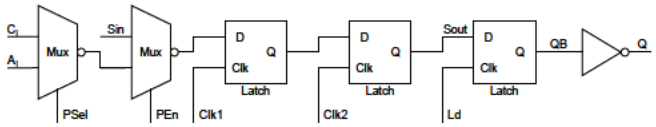

Fig. 9. The structure of the scan flip-flop. A scan flip-flop represents one bit in the shift register. With the first multiplexer and the signal *PSel* one can choose between the counter and adder mode of the readout. [13, sec. 10.1.]

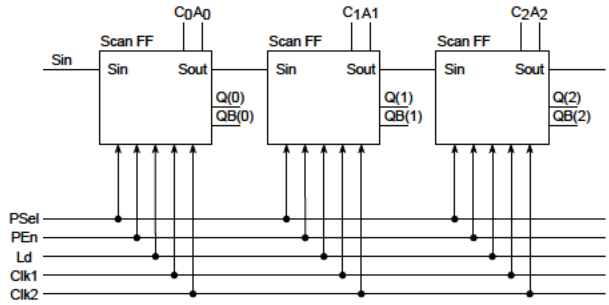

Fig. 10. The connection between the scan flip-flops and the shared control signals. C_i and A_i are the bits of the counter and adder, respectively. The configuration bits Q(i) are used to configure the matrix properties like row address or selection of pixels for injection. [13]

Furthermore, the periphery contains a bias block to generate bias voltages, like the voltages V_1 - V_3 in figures 6 and 7.

III. Characterisation

The measurements performed in our laboratory and at HIT in the beam are presented in this section.

In laboratory, electrical test signals are used to verify general functionality. These test signals are defined voltage steps, applied to the injection capacitance. In this way, a charge signal is produced at the amplifier's input. It can be calibrated by sources with known X-ray energy (e.g. ^{55}Fe). The relation between injection voltage and injected charge is (in a known interval) directly proportional.

A series of injections with increasing charge is used to determine the detection threshold of a pixel. Detection efficiency over injection voltage is not a step function but an error function (integral of Gaussian) due to noise. The inflection point of the error function (c.f. µ of Gaussian) is defined as the detection threshold (50% detection efficiency), the corresponding input referred signal charge is Q_{th}; the transition width of the error function is the noise (c.f. σ of Gaussian).

A common way to get a measure on production induced variations of the response function of individual pixels (transistor mismatch) is the measurement of the distribution of the input-referred threshold.

The signal of charged particles scales with the thickness of the depletion zone of the sensor diode, therefore the maximal depletion voltage before break through has to be determined.

Beam tests are close to the target application of a beam monitor, therefore these measurements are the gold standard. Certain conditions (e.g. particle type and energy, flux, environmental conditions) are not reproducible in laboratory.

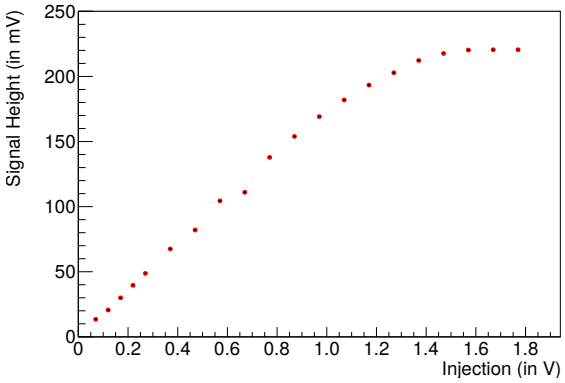

Fig. 11. CSA output signal amplitude versus the injection voltage for HitPixS.

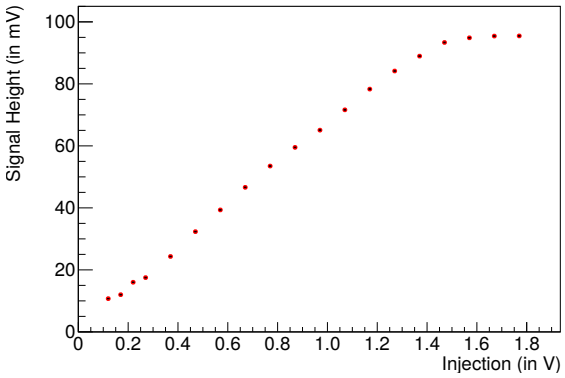

Fig. 12. CSA output signal amplitude versus the injection voltage for HitPixISO.

Most measurements have been repeated on irradiated sensors (various fluences, doses, particle types, annealing periods and irradiation spot shapes).

A. Calibration and threshold scan

HitPixS and HitPixISO allow direct measurements of the output voltage of the CSA. Using the test circuit (capacitor C_{inj} in figure 6), it is possible to inject negative charge into the sensor n-well and imitate particle signals. The injected charge is $Q_{inj} = C_{inj} \cdot V_{inj}$, where V_{inj} is the amplitude of externally generated voltage step signal. Figures 11 and 12 show the CSA output amplitudes versus the injection voltage. The sensitive area (i.e. the sensor diode) – and therefore the pixel capacitance – is larger in case of the HitPixISO. This leads to a lower closed loop gain and therefore a lower charge to voltage conversion gain of the CSA as explained in section II.B. The measurements shown in figures 11 and 12 confirm the expected amplifier gain difference of the two chip flavours.

Figure 13 shows the amplitude distribution of the CSA output signal for X-ray photons generated by an ^{55}Fe source. The data were recorded by connecting an oscilloscope to the amplifier output of a single pixel. The full waveforms were stored and analysed offline. The mean value of the Gaussian fit is 17.81 mV. Comparing the results in figures 13 and 11,

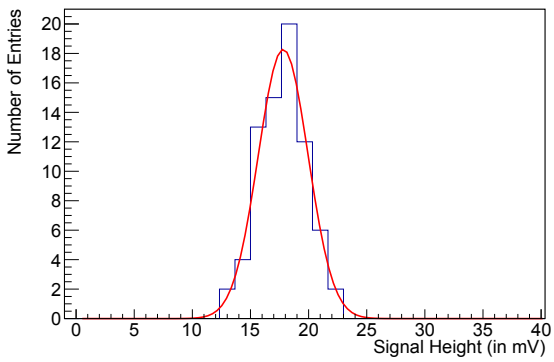

Fig. 13. Histrogram of the CSA output signal amplitudes when the HitPixS sensor is exposed to ^{55}Fe source. The mean signal is 17.81 mV.

we obtain that an injection pulse of about 100 mV generates approximately the same signal at the CSA output as an X-ray photon from an ^{55}Fe source. By taking this into account, and from the known photon energy (5.9 keV for K_α) and average energy needed to produce e-h pairs in silicon, we calculate the injection capacitance C_{inj} to be about 2.7 fF.

Using HitPix as beam monitor, the expected smallest signal amplitude will be in the order of 7 ke^- (for protons with an energy of 220 MeV and a depletion depth of 30 µm) or higher[2]. This is approximately four times the signal from ^{55}Fe. Even in the case of lower gain as in HitPixISO, the output signals will have amplitudes large enough for detection.

In the case of protons, the largest input signals are generated for lowest energies, in our case 60 MeV. From measurements with minimum ionising particles and from stopping power table for protons of 60 MeV, we estimate an average signal of about 27800 e^- (assumption 50 µm depletion) [17, sec. 6.6.1]. The signals are Landau distributed; we expect that 95% of the signals have amplitudes less than three times average. We estimate the smallest signals to about 3500 e^- (50% of the average for 220 MeV protons at 30 µm depletion).

The feedback circuit should discharge the capacitances after amplification of all signals fast enough to avoid analog pile-up, i.e. the input of the comparator should fall below threshold fast enough, to avoid pile-up of consecutive signals. On the other hand, it should generate as little noise as possible, so that smaller signals can also be detected. The linearity of the CSA response, i.e. linear dependence of maximum output voltage versus input charge is not required for this sensor. It is required that particle signals can be counted with frequencies that correspond to maximum particle flux.

Figure 14 shows the simulated response of the HitPixS amplifier to signals of 27800 e^- (4.45 fC) (dashed line) and 3×27800 e^- (solid line).

The feedback circuit has the property that the discharge current increases with longer pulse duration. Therefore, the dead time does not increase linearly with signal amplitude. According to this simulation, counting 60 MeV protons with about 1 MHz is possible. The feedback current can be adjusted

[2]This value has been measured and will be published in a dedicated work evaluating HV-CMOS for ion-beam monitoring.

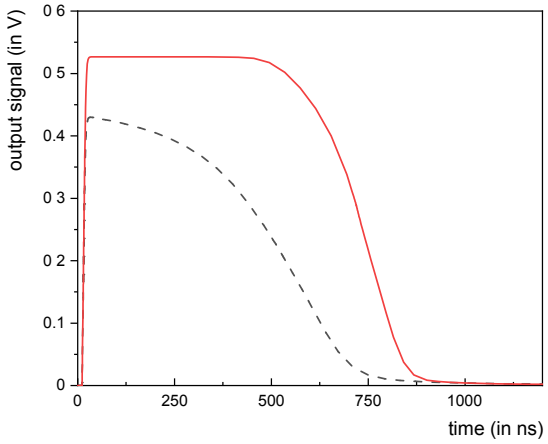

Fig. 14. Simulation of the HitPixS amplifier to an input signal of 27800 e^- (dashed line) and 3×27800 e^- (solid line).

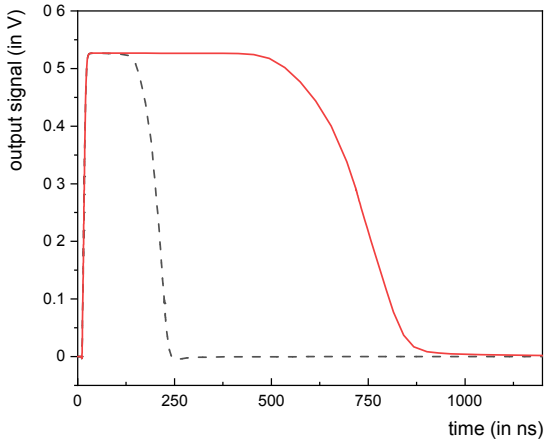

Fig. 15. Simulated signal length for a feedback current of 0.5 nA (solid line) and 2.5 nA (dashed line).

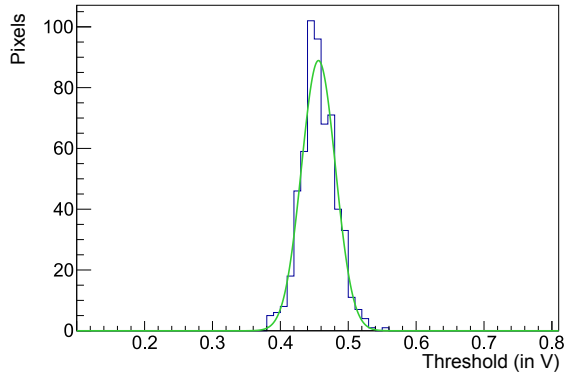

Fig. 16. Histogram of the input-referred threshold Q_{th}, measured with test injections for HitPixS. Q_{th} corresponds to the Q_{inj} leading to the response probability of 50%. The measurement has been performed at 20 °C. The standard deviation of the threshold distribution is 24 mV (390 e^-). [13]

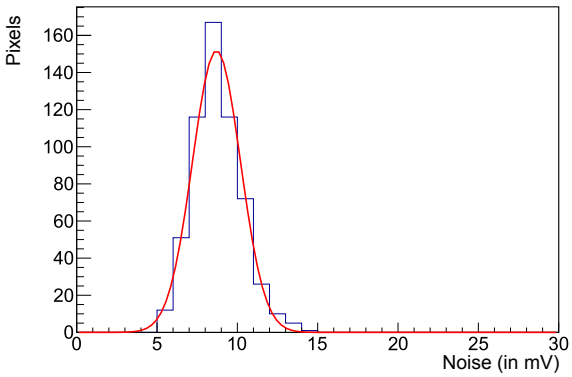

Fig. 17. Histogram of ENC for the pixels on HitPixS. The mean noise is 8.5 mV (140 e^-) with a standard deviation of 1.4 mV (23 e^-). [13]

by on-chip DAC. It was ∼0.5 nA in the simulation. For stronger feedback current, faster reset times can be achieved.

Figure 15 shows the simulated response of a HitPixS amplifier to a 3×27800 e^- signal charge with nominal feedback current of 0.5 nA (solid line) and five times larger feedback current (dashed line).

The simulated equivalent noise charge for the feedback setting of 0.5 nA and without sensor leakage current is 136 e^- for HitPixS and 433 e^- for HitPixIso. This means that the leakage current caused by radiation damage is a significant noise source.

To check the functionality of all pixels in the matrix, we have performed threshold measurements in the following way: Injection pulses are applied to all pixels. The injection amplitude is varied and for each amplitude a constant number of pulses is generated. From the number of signals registered by pixel counters, the response probability is calculated. Noise leads to an error-function-like distribution of the response probability. By fitting the error function to the measured response probability versus the injected charge, the input referred threshold Q_{th} and the equivalent noise charge ENC can be calculated. The measured threshold and noise values differ from pixel to pixel as a result of mismatch between pixel components and supply voltage variations.

Figures 16 and 17 show the histograms of the measured Q_{th} and ENC for HitPixS. Average ENC is 140 e^-. The standard deviation of the threshold distribution translates to 390 e^-.

Figures 18 and 19 show the histograms of the measured Q_{th} and ENC for HitPixISO. Average ENC is 160 e^-. The

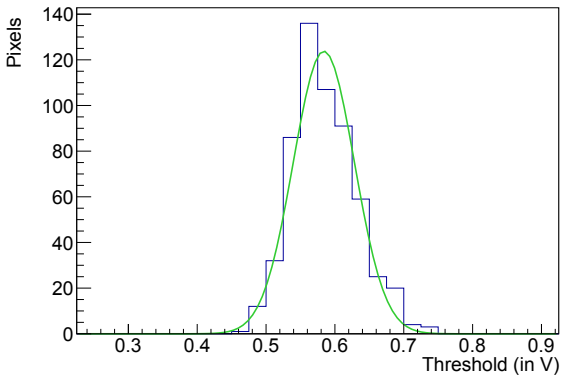

Fig. 18. Histogram of the input-referred threshold Q_{th} for HitPixISO. The standard deviation of the threshold distribution is 44 mV (728 e^-).

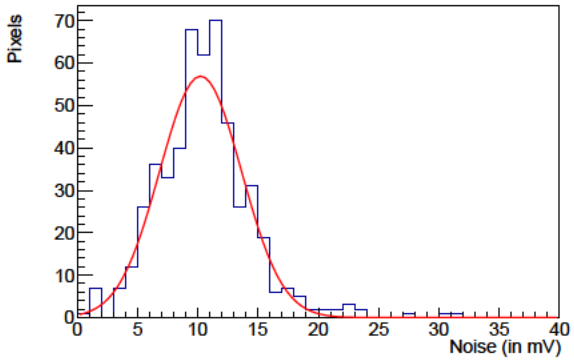

Fig. 19. Histogram of ENC for the pixels of HitPixISO. The mean noise is 10.2 mV ($160\,e^-$) with a standard deviation of 3.4 mV ($56\,e^-$).

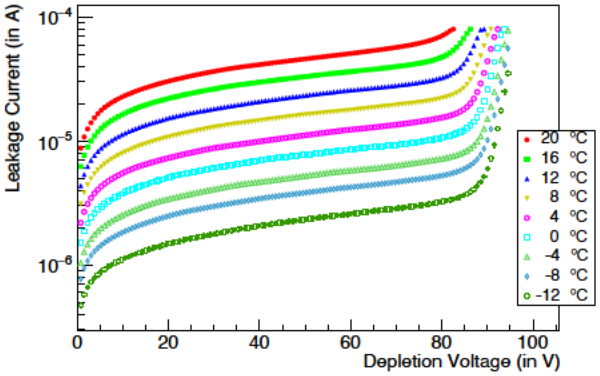

Fig. 20. Temperature dependency of the leakage current measured with HitPixISO irradiated with 25 MeV protons to $1.1 \cdot 10^{15}$ n_{eq}/cm^2.

standard deviation of the threshold distribution translates to $728\,e^-$.

The mean of the threshold distribution is adjustable via Q_{th}.

This matches expectations: Since the electronics is on both flavours identical and noise of an unirradiated chip is dominated by noise sources of the electronics, the measured noise should be similar. The gain (thus signal in V) of HitPixISO is lower compared to HitPixS. The threshold spread is mostly caused by comparator offset variations. This variation is identical in both flavours, thus the variation of input referred thresholds in HitPixISO is larger because the amplifier gain is smaller.

B. Measurements with irradiated sensors

Several HitPixS and HitPixISO chips have been irradiated at KIT [18] with 25 MeV protons up to fluences of $5.0 \cdot 10^{14}$ n_{eq}/cm^2 and $1.1 \cdot 10^{15}$ n_{eq}/cm^2. For technical reasons, we could not measure samples before irradiation, therefore measurements at different fluences are always performed on different samples. The radiation causes bulk damage leading – among others – to an increased sensor leakage current.

The leakage current can be reduced by cooling as shown in figure 20.

The baseline noise at the amplifier output of the HitPixISO before irradiation at 20 °C was measured to be about

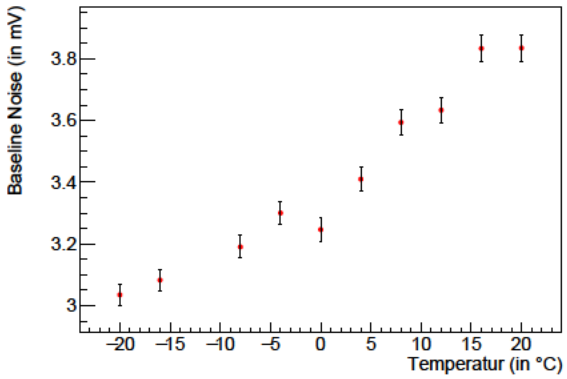

Fig. 21. Measurement of the RMS baseline noise of the irradiated HitPixISO (25 MeV protons, fluence $1.1 \cdot 10^{15}$ n_{eq}/cm^2) at different temperatures.

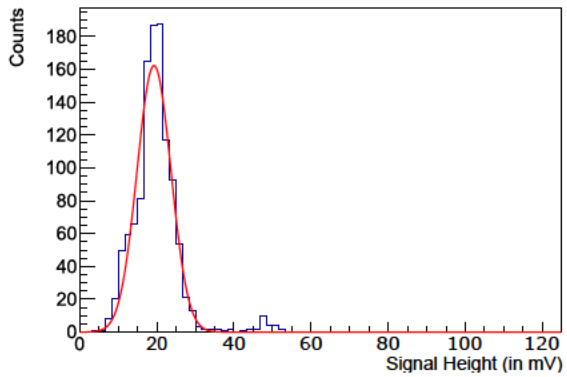

Fig. 22. Histrogram of the CSA output signal amplitudes. Measurement of ^{55}Fe X-rays at -20°C with the HitPixS that was irradiated to the fluence of $1.1 \cdot 10^{15}$ n_{eq}/cm^2 with 25 MeV protons [13]. The measurement time was long, therefore a significant number of noise hits has been recorded and appear in the histogram as entries with higher energy. The mean of the Gaussian fit is 20.05 mV.

3.64 mV (RMS). After irradiation leakage current and shot noise increase. Cooling the sensor is expected to lower the baseline noise caused by leakage current. The measurement of the baseline noise of HitPixISO irradiated with 25 MeV protons to $1.1 \cdot 10^{15}$ n_{eq}/cm^2 at different temperatures shows the expected behaviour (figure 21). A similar result has been obtained with HitPixS.

The restrictions on material budget and homogeneity of the final detector does not allow for cooling structures in the detector. Possibilities are pure passive cooling by environmental air or a forced flow of dried air.

However, cooling reduces noise, enabling the measurement of the very small signal of ^{55}Fe. The signals from an ion-beam are much larger and no cooling to temperatures below room temperature is required to detect them.

Signals from ^{55}Fe were recorded with an irradiated HitPix at -20 °C. The average signal amplitude is 20.05 mV as shown in figure 22, it matches the result of the unirradiated sensor. The chip was cooled down to reduce noise and leakage current. The baseline noise was about 2.8 mV (RMS) at this temperature.

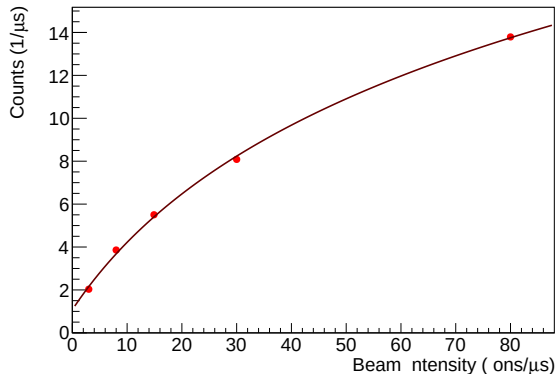

Fig. 23. Counting rate versus beam intensity, measured with a HitPixS in the beam test at HIT.

C. Beam Measurements

Several beam tests have been performed at Heidelberg Ion-beam Therapy Center (HIT). The beam intensity, particle type (protons or carbon ions) and energy have been varied.

Figure 23 shows the counting rate for different beam intensities. The shown data have been measured with an carbon ion-beam with a FWHM diameter of 3.3 mm directed to the mid of the sensor. The pixel response is not uniform. This effect originates from charge sharing in combination with mismatch. Production variations give each pixel a unique amplification and detection threshold, resulting in more or less sensitive pixels. The signal charge of the ion-beam is large enough to be detected by any threshold and any amplification. However, often the signal charge is not collected in a single pixel, but the charge is shared by two or more. In this case, pixels with lower sensitivity might not detect the particle, while a more sensitive pixel detects the particle. This inhomogeneity will be addressed by implementing an adjustable threshold in each pixel (tune-DAC) in the next HitPix iteration.

In this configuration, we calculate that 2/3 of the beam particles have to pass the sensor (c.f. figures 24 and 26). For low intensities the counting rate matches the expectation, for higher rates the dependency becomes sub-linear. This can be explained by pile-up of signals at the CSA output. This problem will be addressed in the next sensor version, for example by increasing the feedback current I_f in figure 6.

Figure 24 shows the image of the carbon ion-beam obtained with pixel counters (measured on HitPixS). The beam intensity was $2 \cdot 10^6$ carbon ions/s at an energy of 423.44 MeV/u. The adders at the end of each column allow measurement of the beam projection as shown in figure 25.

Figure 26 shows the image of the carbon ion beam obtained with HitPixISO. The beam intensity was $2 \cdot 10^6$ carbon ions/s at an energy of 430.10 MeV/u.

IV. Conclusion

We are developing a silicon beam monitor for ion-beam therapy. The beam monitor could contain 2 layers, 25 cm $\times$ 25 cm in size, containing approximately 170 sensor chips each. We have designed and tested the HV-CMOS

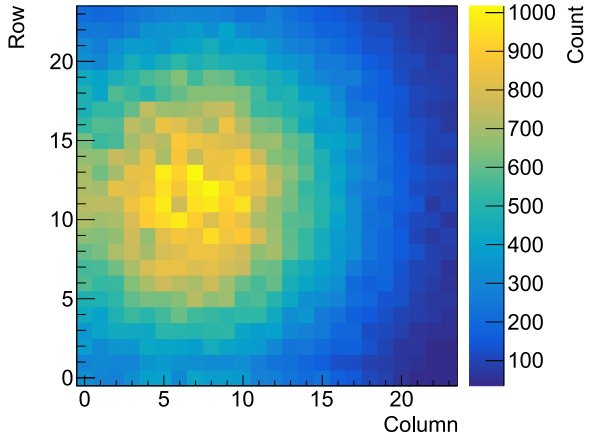

Fig. 24. Integrated counts of the pixels displaying the spot of the carbon beam $2 \cdot 10^6$ carbon ions/s at an energy of 423.44 MeV/u. Measured on HitPixS.

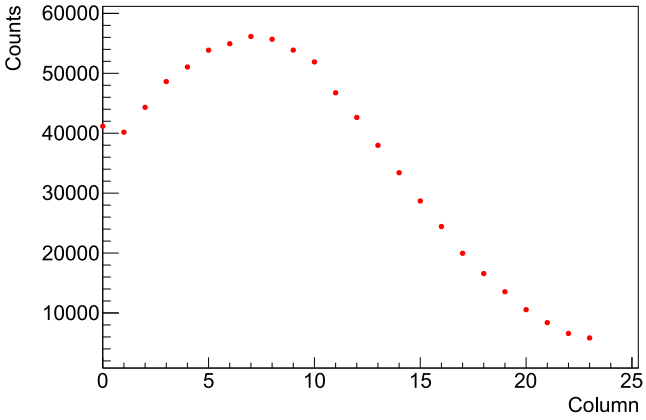

Fig. 25. In adder readout mode, the sum of all counter states per column is read out. The result is a projection. The graph shows the profile of a carbon beam with $2 \cdot 10^6$ ions/s at an energy of 423.44 MeV/u, measured by HitPixS.

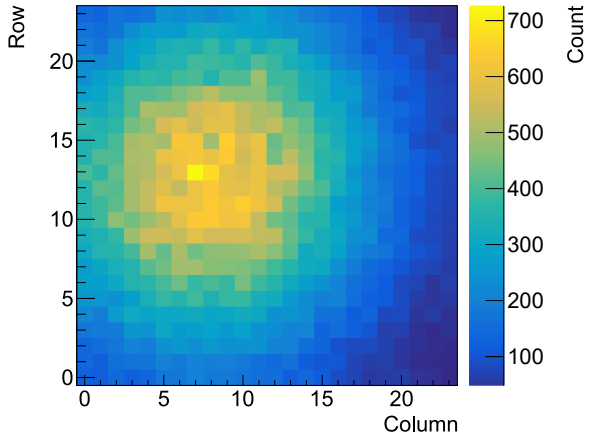

Fig. 26. Integrated counts of the pixels displaying the spot of the carbon beam $2 \cdot 10^6$ carbon ions/s at an energy of 430.10 MeV/u. Measured on HitPixISO.

monolithic active pixel sensor prototype HitPix with counting pixel electronics for beam monitoring. The sensor area is about 5 mm × 5 mm. The pixel size is 200 µm × 200 µm. The sensor has been implemented in a commercial HV-CMOS technology on high-resistive substrate. Two sensor flavours have been realised and used: One with pixel electronics inside the sensor cathode (HitPixISO) and one with sensor and electronics in separate n-wells (HitPixS). HitPixISO uses an additional deep p-well for isolation between the n-wells. Functionality of both flavours has been confirmed by laboratory test including source measurements and detection threshold scans and have been used to measure the beam profile at the Heidelberg Ion-beam Therapy Center.

In 2021, HitPix2 has been designed and submitted. It has arrived in Dec. 2021 and is currently being characterised. HitPix2 has a size of about 1 cm × 1 cm with 48 × 48 pixels. The electronics is very similar to the one used in the first generation. It was designed with separated n-wells (HitPixS flavour).

At the moment, the design of the HitPix3 is ongoing. There, the amplifier will be modified to minimise an alog pile-up. Furthermore, a second adder in each pixel will enable the row projection to get a beam profile in both directions. A decision of flavour has not yet been made. This and other final design decisions depend on further beam test results with HitPix and HitPix2.

ACKNOWLEDGMENTS

We would like to thank our colleagues from the Heidelberg Ion-beam Therapy Center, especially Jakob Naumann for the help and support during beam measurements.

REFERENCES

[1] Heidelberg University Hospital, "Proton Therapy and Carbon Ion Therapy.", https://www.heidelberg-university-hospital.com/diseases-treatments/cancer-and-tumor-diseases/proton-therapy-and-carbon-ion-therapy, Accessed: Jan. 2022.

[2] I. Perić, "A novel monolithic pixel detector implemented in high-voltage CMOS technology." *2007 IEEE Nuclear Science Symposium Conference Record*, 2007, pp. 1033-1039, doi: 10.1109/NSSMIC.2007.4437188.

[3] J. Meikle, "How particles can be therapeutic." https://physicsworld.com/a/how-particles-can-be-therapeutic, 2003, Accessed: Aug. 2020.

[4] M. Torikoshi et al., "Continuous Beam Monitoring for Charged Particle Therapy.", *Proceeding of the 10th symposium on accelerator science and technology* (JAERI-Conf–95-021), Oct. 1995.

[5] ATLAS Collaboration, "Technical Design Report for the ATLAS Inner Tracker Pixel Detector", No. CERN-LHCC-2017-021. ATLAS-TDR-030, Sep. 2017.

[6] CMS Collaboration, "The CMS experiment at the CERN LHC", *Journal of Instrumentation*, vol. 3, p. S08004, Aug. 2008, doi: 10.1088/1748-0221/3/08/s08004.

[7] I. Perić et al., "High-Voltage CMOS Active Pixel Sensor." *IEEE Journal of Solid-State Circuits*, vol. 56, no. 8, pp. 2488-2502, 2021, doi: 10.1109/JSSC.2021.3061760.

[8] T. Rudzki et al., "The Mu3e experiment: Toward the construction of an HV-MAPS vertex detector," *arXiv* 2021, arXiv:2106.03534.

[9] F. Ehrler, "Characterization of monolithic HV-CMOS pixel sensors for particle physics experiments", PhD thesis, Karlsruhe Institute of Technology, Apr. 2021, doi: 10.5445/IR/1000133748.

[10] D. Ondreka and U. Weinrich, "The Heidelberg Ion Therapy (HIT) Accelerator Coming into Operation", *EPAC08 Proceedings*, pp. 979-981, 2008.

[11] F. Ehrler, "Development of active CMOS sensors for particle physics experiments." Master thesis, Karlsruhe Institute of Technology, Nov. 2015, doi: 10.5445/IR/1000055062.

[12] G. Borghello, "Ionizing radiation effects in nanoscale CMOS technologies exposed to ultra-high doses." PhD thesis, University of Udine, Oct. 2018.

[13] A. Weber, "Development of Integrated Circuits and Smart Sensors for Particle Detection in Physics Experiments and Particle Therapy." PhD thesis, Heidelberg University, Oct. 2021.

[14] G. Anelli et al., "Radiation tolerant VLSI circuits in standard deep submicron CMOS technologies for the LHC experiments: practical design aspects." *IEEE Trans. Nucl. Sci*, vol. 46, no. 6, pp. 1690-1696, Dec. 1999, doi: 10.1109/23.819140.

[15] L. Dong-Mei et al., "Study of total ionizing dose radiation effects on enclosed gate transistors in a commercial CMOS technology." *Chin. Phys. B*, vol. 16, no. 12, pp. 3760-3765, 2007, doi: 10.1088/1009-1963/16/12/034.

[16] W. Snoeys et al., "Layout techniques to enhance the radiation tolerance of standard CMOS technologies demonstrated on a pixel detector readout chip." *Nucl. Instrum. Methods A*, vol. 439, no. 2, pp. 349-360, 2000, doi: 10.1016/S0168-9002(99)00899-2.

[17] R. Schimassek, "Development and Characterisation of Integrated Sensors for Particle Physics", PhD thesis, Karlsruhe Institute of Technology, Dez. 2021, doi: 10.5445/IR/1000141412.

[18] KIT ETP, "Bestrahlungszentrum Karlsruhe." https://www.etp.kit.edu/Bestrahlungszentrum.php, Accessed: Sep. 2021.